Using instability of a nonstoichiometric mixed oxide oxygen evolution catalyst as a tool to improve its electrocatalytic performance

Olga Kasian[a,*], Simon Geiger[a], Maximilian Schalenbach[a], Andrea M. Mingers[a], Alan Savan[b], Alfred Ludwig[b], Serhiy Cherevko[a,c], Karl J. J. Mayrhofer[a,c,d]

[a]*Max-Planck-Institut für Eisenforschung GmbH, Max-Planck-Straße 1, 40237 Düsseldorf, Germany*

[b]*Institute for Materials, Ruhr-Universität Bochum, 44801 Bochum, Germany*

[c]*Helmholtz-Institute Erlangen-Nürnberg for Renewable Energy (IEK-11), Forschungszentrum Jülich, Egerlandstr. 3, 91058 Erlangen, Germany*

[d]*Department of Chemical and Biological Engineering, Friedrich-Alexander-Universität Erlangen-Nürnberg, Egerlandstr. 3, 91058 Erlangen, Germany*

Tel: +49 (211) 6792-160; Fax: +49 (211) 6792-218

E-mail: o.kasian@mpie.de

Abstract

Owing to their superior electrocatalytic performance, non-stoichiometric mixed oxides are often considered as promising electrocatalysts for the acidic oxygen evolution reaction (OER). Their activity and stability can be superior to those of the state-of-the-art IrO_2 catalyst, although the exact nature of this phenomenon is not yet understood. In the current work a $Ir_{0.7}Sn_{0.3}O_{2-x}$ thin-film electrode is taken as a representative example for a thorough evaluation of OER activity of the non-stoichiometric oxides. Complementary activity and stability analysis of $Ir_{0.7}Sn_{0.3}O_{2-x}$ electrodes is achieved using a setup based on an electrochemical scanning flow cell and ICP-MS. The obtained ICP-MS data presents an unambiguous proof of the preferential dissolution of the less noble Sn from the mixed oxide during OER. While less than a monolayer of Ir is dissolved after a prolonged electrolysis of 1400 min during which its dissolution rate drops to near zero, the amount of Sn lost is ten monolayers. The latter finding is confirmed by XPS analysis, which besides showing Ir surface enrichment also indicates a gradual transformation of Ir^0 to Ir^{III} species. This transition is beneficial for electrode activity, as the overpotential for OER at $j = 5$ mA cm^{-2} was decreasing up to 300 mV. The increase in electrode activity is attributed to several mechanisms including generation of Ir^{III} active sites and overall surface area increase. A generalized description of OER catalysis by Ir-based materials is given, including data from the current work as well as from other Ir-based mixed oxides, such as Ir-Ru-O and Ir-Ni-O.

1

2

4

5

1   **Introduction**

2

3   The oxygen evolution reaction (OER) is the counter reaction in numerous industrially important processes,

4   such as electrochemical hydrogen production, cathodic electrosynthesis, metal electrowinning, etc. [1]. Even though

5   in some of these applications the use of mature, non-noble metal based electrodes such as PbO_2 can be justified [2, 3],

6   all of them would benefit from the development of a more active alternative. Electrode stability, however, should not

7   be sacrificed. Considering acidic environments as the most promising ones, nowdays only Ir-based anodes meet these

8   strict requirements [4-7]. Scarcity and the high price of Ir, however, are serious hinderances in the way of its universal

9   application. Hence, optimization of the catalyst utilization becomes of very high importance. There are several options

10   given in the literature for how this can be achieved. Among them, the increase in surface area of Ir-based catalysts by

11   using nanoparticles [8] or porous structures [9, 10] is the most-used approach for improving the gravimetric

12   electrocatalytic activity. Another possibility is dilution of Ir by alloying with other metals. The representative

13   examples here are the systems in which Ir is alloyed with electrochemically less stable metals, e.g. Ir-Ru [11-14] and

14   Ir-Ni mixed oxide [10] or Ir based perovskites [15, 16], which sometimes show higher activity than Ir oxide. As a rule,

15   however, improved electrocatalytic activity of these compounds is counterbalanced by their lower stability towards

16   dissolution. In these systems, dissolution of the less stable component usually occurs together with an increased

17   dissolution of Ir, resulting in the overall catalyst instability [10, 14]. On the other hand, mixing of Ir oxide with

18   significanlty less active but more stable materials e.g. Ti [17] or Sn [18] typically results in catalysts showing very

19   high stability against dissolution. In this case, however, deterioration of electrocatalytic performance with time is to be

20   expected, taking into account semiconducting nature of stoichiometric TiO_2 and SnO_2 [19-21].

21   In achieving a compromise between activity and stability, non-stoichiometric oxides of Ir and more stable

22   elements can be considered as very promising catalyst materials [22]. In such compounds, oxygen vacancies can serve

23   as the active sites for the OER [23]. At the same time, owing to the their high thermodynamic stability, longevity of

24   Ir-Sn and Ir-Ti-based non-stoichiometric oxides during the OER can be still sufficiently high for their successful

25   commericalization. Before that is accepted as a viable approach however, a thorough analysis concerning their activity

26   and stability is required. While the former is easy to be addressed by common electrochemical methods, the latter

27   requires a more comprehensive investigation since the literature lacks in insight into the stability and degradation

28   mechanisms of Ir-based non-stochiometric mixed oxides.

29   In the current work, non-stoichiometric $Ir_{0.7}Sn_{0.3}O_{2-x}$ is chosen as a representative example in order to evaluate

30   the applicability of this class of materials for catalysing acidic OER. The oxide is prepared using reactive sputtering as

1   a technique allowing one to precisely control elemental composition and degree of stoichiometry. Activity and

2   stability are investigated in parallel by a scanning flow cell (SFC) connected to an inductively coupled plasma mass

3   spectrometer (ICP-MS). This allows the precise separation and indification of partial dissolution rates of Ir and Sn and

4   their correlation with electrochemical surface processes. Changes in the electrode composition and electronic

5   properties triggered by dissolution are analysed and their effect on electrode performance is studied and discussed.

6

7   **Experimental**

8

9   Thin $Ir_{0.7}Sn_{0.3}O_{2-x}$ films were deposited by confocal reactive co- sputtering (Creavac, Dresden, Germany). To

10   prepare films with a minimal surface roughness, smooth substrates of single crystalline Si(100) wafers with a 1.5 μm

11   thermal SiO_2 diffusion and reaction barrier layer were used. The base vacuum before deposition was 2.5×10^{-6} Pa. The

12   Ø2 inch target of Sn (99.95%, EvoChem, Germany) and Ø4 inch target of Ir (99.9%, Evochem, Germany) were pre-

13   cleaned by sputtering against closed shutters prior to deposition. A mixture of O_2 and Ar was used as the sputter gas

14   and the chamber pressure was regulated to 0.66 Pa at room temperature. Ir and Sn were deposited simultaneously at

15   85 W DC and at 30 W DC, respectively. The resulting thickness of the obtained coating was approximately 200 nm.

16   The composition of the film was confirmed using energy dispersive X-ray analysis (EDX, INCA X-act, Oxford

17   Instruments, U.K.) and X-ray photoelectron spectroscopy (XPS) and can be described as $Ir_{0.7}Sn_{0.3}O_{2-x}$ (where 0<x<2).

18   XPS measurements were carried out (Quantera II, Physical Electronics, Chanhassen, MN, USA) applying a

19   monochromatic Al Kα X-ray source (1486.6 eV) and operating at 15 kV and 25 W. The binding energy scale was

20   referenced to the C 1s signal at 285.0 eV. Casa XPS software was used to analyze the experimentally obtained spectra.

21   The fitting of spectra was performed after subtraction of a Shirley background. In all fits, the peak separation and the

22   peak area ratios between the Ir 4f7/2 and the Ir 4f5/2 components were constrained to 3 eV and 4:3, respectively. A

23   Doniach-Šunjic profile with an asymmetry parameter of 0.1 and a spectrum convolution width of 100 was used for the

24   peak fittings. Detailed discussion of Ir XP spectra interpretation can be found in the literature [24-26].

25   The prepared $Ir_{0.7}Sn_{0.3}O_{2-x}$ thing films served as the working electrode in the scanning flow cell– inductively

26   coupled plasma mass spectrometer (ICP-MS, NexION 300X, Perkin Elmer) based setup SFC-ICP-MS, as described in

27   [5, 27]. All presented data are normalized to the geometric area of the working electrode (1×10^{-2} cm^2) assuming low

28   roughness of the sputtered films. A graphite rod, placed in the inlet channel of the SFC, was utilized as the counter

29   electrode. A saturated Ag/AgCl electrode (Metrohm, Germany) was used as the reference electrode. All reported

30   potentials are referenced to the reversible hydrogen electrode (RHE) potential, that was measured in each day of

31   experiments using a polycrystalline platinum foil (99.99%, MaTeck, Germany) in hydrogen saturated 0.1 M $HClO_4$.

1   This solution was prepared by dilution of concentrated acid (Suprapur® 70% $HClO_4$, Merck, Germany) in ultrapure

2   water (PureLab Plus system, Elga, 18 MΩcm, TOC < 3 ppb) and, after saturation with Ar, was also used in all

3   electrochemical measurements. A potentiostat (Gamry Reference 600, USA) was used for the electrochemical

4   measurements.

5   Prior to introduction into the ICP-MS the electrolyte was mixed with an internal standard in a Y-connector

6   (mixing ratio 1:1) after the electrochemical cell. As internal standards for detection of ^{118}Sn and ^{193}Ir isotopes, 10 μg

7   L^{-1} of ^{103}Rh and ^{187}Re were used, respectively. The ICP-MS was calibrated every day of experiment prior to the

8   electrochemical measurements.

9   Long-term stability measurements were performed using an h-cell with anodic and cathodic compartments

10   divided by a fine glass frit (Pine Research Instrumentation, USA). The volume of electrolyte in the anodic and

11   cathodic compartments was adjusted to 20 mL and kept constant during the measurements. A Pt foil and saturated

12   Ag/AgCl positioned in the same compartment were used as counter and reference electrodes, respectively.

13   In the stability – OER activity studies, the following experimental protocol was used. The working electrode

14   was polarized at E = 1.20 V_{RHE} during 2 min. for initial stabilization. Afterwards, the potential of the electrode was

15   swept from E = 1.20 V_{RHE} to a value corresponding to a current density j = 5 mA cm^{-2} with a scan rate of 10 mV s^{-1}.

16   Then, the electrode was polarized at 1 mA/cm^2 for 10, 30 or 60 min. After that, an identical potential sweep was

17   performed again in order to understand the change in electrochemical behavior of the electrode material after anodic

18   polarization. All measurements were reproduced at least three times.

19

20   **Results**

21

22   *X-ray photoelectron spectroscopy*

23

24   XPS has been effectively applied as both an ex-situ and in-situ surface-sensitive technique in numerous

25   studies of pristine or mixed Ir-based oxides for OER [12, 14, 25, 28, 29]. It provides information about the chemical

26   state and ratio between elements in as-prepared materials and even more importantly on the change in the composition

27   during anodic polarization. In this context, XPS was used in the current study. XP spectra of Ir 4f, Sn 3d and O 1s

28   levels before (top curves) and after (bottom curves) anodic polarization are represented in Figs. 1a, 1b and 1c,

29   respectively. According to the obtained results, the as-prepared sample contains 70 at.% of Ir and this value increases

30   to almost 85 at.% after the anodic polarization. Independent on the electrochemical pretreatment, the Sn 3d peak is

31   centered at ca. 486.9 eV, mainly corresponding to the oxidation state Sn^{IV} [30, 31]. However, taking into account the

1   similar binding energies for SnO and SnO_2, the presence of SnO on the surface of the as-prepared electrode cannot be

2   excluded [30]. Detailed analysis of Ir 4f spectra in the as-prepared material (Fig. 1a, top line) allows resolving and

3   quantifying two components corresponding to IrO_2 (61.6 eV) [14, 25] and metallic Ir (60.6 eV) [32] in the atomic

4   ratios of ca. 60 to 40 percent, respectively. There is a drastic change in the spectrum of the Ir 4f level after the

5   electrode is treated anodically during the OER. Instead of the metallic phase, Ir^{III} species appear at 62.2 eV [9, 26] in

6   an amount of ca. 30 at.% (Fig. 1a, bottom line). Apparently, anodic polarization leads to complete transformation of

7   metallic Ir into Ir^{III} and Ir^{IV}.

8   The O 1s spectra for the as-prepared and electrochemically pretreated electrodes are presented in Fig. 1 c (top

9   and bottom curves, respectively). Three well-resolved components corresponding to O in the oxide lattice (530.5 eV),

10   O from OH groups (531.6 eV) and water (532.5 eV) can be identified in the spectra. Electrochemical treatment does

11   not affect the positions of the corresponding peaks. According to these results, in the as-prepared sample lattice

12   oxygen dominates in the O 1s spectrum, while after anodic polarization an increase in the contribution of OH/O and

13   H_2O/O is found. A similar effect was observed in the case of IrO_2-RuO_2 mixed oxides [14].

14

15   *Oxygen evolution and electrochemical dissolution of $Ir_{0.7}Sn_{0.3}O_{2-x}$ electrode*

16

17   For the electrochemical characterization, the potential of an as-prepared $Ir_{0.7}Sn_{0.3}O_{2-x}$ electrode was swept into

18   the anodic direction with the scan rate of 10 mV s^{-1} from 1.2 V_{RHE} until the potential reached the value corresponding

19   to a current density of 5 mA cm^{-2}. This was followed by anodic polarization at 1 $mAcm^{-2}$ for 10, 30 or 60 minutes.

20   Afterwards, an identical potential scan was carried out in order to investigate if the anodic treatment had an effect on

21   electrode activity and stability. The quasi-steady-state anodic polarization curves are presented in Fig. 2a. With an

22   increase in anodic polarization time, the overpotential of the OER tends to decrease. Already after 30 min. it reaches a

23   value close to that of stoichiometric IrO_2. Moreover, the electrode treated for 60 min. has ca. 100 mV lower

24   overpotential at j = 5 mA cm^{-2} (comparing curves 3 and 5 in Fig. 2a). Further increase in anodization times results in

25   only a slight increase in activity. In order to understand the origin of the increased activity of the anodically treated

26   electrodes, cyclic voltammograms (CV) before and after anodic polarization were recorded (see Fig. 2b for as-

27   prepared and 60 min. polarized $Ir_{0.7}Sn_{0.3}O_{2-x}$ electrodes). Comparing the two, one can see that the anodic treatment

28   results in the appearance of two broad waves in the anodic and cathodic branches of the CV at ca. 0.95 and 0.65 V_{RHE},

29   respectively. These features can be assigned to the Ir(IV)/Ir(III) transitions that are typically observed in the CVs of

30   hydrous or amorphous iridium oxides [5, 33]. The double layer charging current is also increased, which may indicate

31   a slight increase in the electrode's surface area.

1   In parallel with the above-described electrochemical procedure, dissolution profiles of Ir and Sn were taken

2   (Fig. 3). During both potential sweep and steady-state polarization regimes the rate of Sn dissolution significantly

3   exceeds the rate of Ir dissolution. A similar trend in dissolution was also observed in the case of Ir–Ru and Ir–Ni

4   mixed oxides [10, 14]. The onset of Ir dissolution is ca. 1.56 V_{RHE}, while Sn already starts dissolving at the open

5   circuit potential. One can see from Fig. 3c that dissolution of both elements decreases after anodic polarization.

6   The total amounts of Ir and Sn dissolved during 10, 30 and 60 min. of the OER in galvanostatic conditions in

7   the SFC were obtained by integrating the corresponding dissolution profiles and the data is shown in Fig. 4 (opened

8   symbols). Both curves show similar decreases in the rate of dissolution with time. The highest dissolution rate was

9   observed in the first minutes. Thus, during the first 10 min. of oxygen evolution the amount of dissolved Ir was about

10   5 ng cm^{-2}. For comparison, at exactly same conditions of anodic polarization ca. 2 ng cm^{-2} of Ir dissolves from the

11   IrO_2 anode, indicating a relatively lower stability of the mixed oxide. In addition, the amount of lost Sn was 32 ng cm^{-}

12   ^{2}. Comparison of Fig. 3c and d shows decrease in dissolution rates from 0.012 to 0.008 ng $cm^{-2} s^{-1}$ and from 0.1 to

13   0.04 ng $cm^{-2} s^{-1}$ of Ir and Sn, respectively.

14   Typical operational times of SFC-ICP-MS are limited to few hours. In order to examine the longer-term

15   stability of the anode, galvanostatic measurements were performed in the h-cell with divided anodic and cathodic

16   compartments. To do so, aliquots of 1 mL were taken periodically from both compartments and further analyzed using

17   the ICP-MS. The amount of Ir in both compartments was below the detection limit after the first 30 min. of

18   measurements owing to the high volume of the cell. Moreover, no Ir was detected in the cathodic compartment during

19   the entire experiment, while the amount of Sn in the cathodic compartment never exceeded 5% of the concentration of

20   Sn in the anodic compartment. Both concentrations were considered to estimate dissolution. The measurements were

21   stopped when the change in the concentration for both elements was lower than 9% in 10 hours, which is an indication

22   that quasi steady state is achieved. The steady-state dissolution rates of Ir and Sn approached the values of 0.0001 ng

23        $cm^{-2} s^{-1}$ and 0.0005 ng $cm^{-2} s^{-1}$, respectively. The results obtained in the h-cell are shown in Fig. 4 by solid symbols.

24   One can see that there is good agreement between the data obtained in two setups. Hence, owing to its high

25   sensitivity, SFC-ICP-MS can be considered as a powerful tool for determining the initial dissolution rates, which is

26   extremely important in noble metals dissolution kinetics studies. These values can be useful for estimation of

27   dissolution in the flow reactors, where equilibrium is not necessarily to be achieved. On the other hand, h-cell

28   measurements are complementary providing valuable information on equilibrium concentration of the dissolved

29   elements.

30

31   **Discussion**

1

2   It is anticipated that oxygen deficiency in an oxide material can be desirable in terms of catalytic activity

3   [34]. In particular, catalytically active sites for the OER are often associated with oxygen vacancies [23]. The impact

4   of oxygen vacancies on the OER can be ascribed to the dependence of both chemical potential and surface potential

5   on the degree of ionicity and non-stoichiometry [35]. Lattice defects in the bulk as a rule modify the chemical

6   potentials of the compound, while surface defects effect the local charge distribution and, as a result, surface potential.

7   Availability of such defects and their high concentration in a catalyst can additionally facilitate the reaction at lower

8   temperatures owing to a decrease in the activation energy of adsorption step [35]. However, owing to poor

9   electrocatalytic properties of the Sn-containing electrode surface and semiconducting nature of tin oxides, the initially

10   prepared $Ir_{0.7}Sn_{0.3}O_{2-x}$ anode has a relatively high OER overpotential. During the OER, electrocatalytic activity of the

11   $Ir_{0.7}Sn_{0.3}O_{2-x}$ anode tends to increase with time (Fig. 2a). A similar trend was reported recently by Reier et. al. for the

12   Ir-Ni system [10]. This behavior can be understood by taking a closer look at the XPS data. It reveals that after anodic

13   polarization the Ir to Sn ratio increases. Moreover, the analysis of the Sn 3d spectra from the as-prepared and treated

14   electrodes presented in Fig. 1b shows further that the electrode near surface layer consists of oxide (either Sn^{II} or Sn^{IV}

15   or a mixture of both) but not metallic Sn. Since dissolution of SnO_2 should not be observed at these conditions [36], a

16   conclusion can be made that thermodynamic instability of SnO is responsible for the relatively high initial dissolution

17   of Sn (Fig. 3). Unlike Sn, some amount of metallic Ir is present in the as-prepared film. With anodic polarization,

18   however, conversion of metallic Ir to Ir^{III} and Ir^{IV} species takes place. Owing to their lower coordination number, Ir^{III}

19   species can themselves be responsible for the observed electrocatalytic activity improvement [9, 10, 26, 28, 37]. It is

20   expected that adsorption of oxygen containing radicals on Ir^{III} will be stronger than on Ir^{IV}, and, therefore, favorable.

21   The increase in OH groups and H_2O contribution in the overall O1s spectra presented in Fig. 1c suggests formation of

22   a porous structure and a change in hydrophilicity of the oxide. Hence, it may be concluded that a process similar to

23   dealloying takes place at the electrode during the OER. As was discussed by Debe, the latter is typically responsible

24   for the resulting increased surface area of the electrocatalyst [38]. Indeed, according to Fig. 2b, the surface area of the

25   $Ir_{0.7}Sn_{0.3}O_{2-x}$ electrode is increasing in time owing to intensive removal of one of the components. Thus, there are at

26   least two or three mechanisms contributing to the activity enhancement: (a) formation of Ir^{III} active sites and (b)

27   surface area increase and (c) removal of the less active component. The contribution of each of them is, however,

28   difficult to differentiate. It is anticipated that the change in the electronic structure also influences electronic

29   conductivity. Interestingly, no increase in catalytic activity was reported for Sn – noble metal based mixed oxides,

30   prepared by thermal decomposition of respective salts in air [21]. As a rule, stoichiometric SnO_2 is formed in this

31   case, which is related to a relatively high affinity of Sn for oxygen.

1   High electrocatalytic activity is important but not the only parameter to be expected from a good OER

2   electrocatalyst. Even the most active material has no future application if it cannot guaranty a stable long-term

3   electrolyser performance. Hence, dissolution results should also be discussed. In line with the Ir and Sn XP spectra

4   change, SFC-ICP-MS data shows much higher dissolution rates of Sn in comparison to Ir (Fig. 3). Already during the

5   first potential ramp in the anodic direction, dissolution of Ir from the $Ir_{0.7}Sn_{0.3}O_{2-x}$ anode was higher than that for IrO_2.

6   Several explanations can be given for this phenomenon. As shown in Fig.1, $Ir_{0.7}Sn_{0.3}O_{2-x}$ consists of ca. 40 at.% of

7   metallic Ir, which is significantly less stable towards dissolution in comparison to rutile IrO_2 [39]. Additionally, the

8   poor catalytic activity of the as-prepared $Ir_{0.7}Sn_{0.3}O_{2-x}$ means that a higher overpotential is required to achieve the

9   same current density. Considering that electrochemical dissolution increases with potential, the lower stability is to be

10   expected. It should be noted, however, that SnO_2 is a relatively poor electronic conductor (semiconductor), which

11   means that some potential drop may take place in the catalyst itself. Hence, the potential at the outer Helmholtz plane

12   can be significantly lower. Interestingly, during the first 30 min. of anodic polarization about 18 ng cm^{-2} of Ir is

13   dissolved from $Ir_{0.7}Sn_{0.3}O_{2-x}$, which is similar to that observed in the Ir-Ni system with 70 at.% of Ir [10]. This can be

14   an indication of similar kinetics of initial Ir dissolution for both materials. However, data on the dissolution rates

15   during long term polarization of Ir-Ni mixed oxide anodes is not found in the literature.

16   Dissolution rates of both Ir and Sn decrease with time as seen in Figs. 3c,d. A similar trend is observed in the

17   long-term measurements (Fig. 4). However, decrease in dissolution rates observed in these two setups has different

18   origin. In a flow cell dissolution decreases because of the change in the electrode surface composition during the

19   galvanostatic treatment. In a bulk cell along with surface composition changes, accumulation of dissolution products

20   occurs until steady state or equilibrium concentration is achieved.

21   Using the data on the covalent radii of Ir and Sn and densities of the corresponding oxides together with our

22   dissolution data, one can calculate the number of monolayers dissolved from $Ir_{0.7}Sn_{0.3}O_{2-x}$ anode during anodic

23   polarization. Thus, during the first 10 min. of electrolysis the amount of dissolved Sn and Ir corresponds to about 70%

24   and 2% of a monolayer, respectively. After 60 min., these numbers increase to 5 monolayers and 10% of a monolayer,

25   respectively. Anodic treatment of electrode during 1400 min. led to removal of Sn from almost 10 monolayers while

26   the dissolution of Ir was still below a monolayer.

27   Results presented in the current work can be analyzed together with those published previously for Ir-Ru [14]

28   and Ir-Ni mixed oxides [10]. This analysis reveals that if a less stable oxide is mixed with Ir, it still undergoes

29   dissolution under the OER conditions, leading to formation of a porous Ir structure. When IrO_2 is mixed with RuO_2,

30   which is a more active OER electrocatalyst, the overall electrocatalytic performance of the electrode deteriorates with

31   time and reaches what is expected for pure IrO_2. On the other hand, activity of Ir-Ni and Ir-Sn mixed oxides gets

1 better with time, which as discussed above can be related to the increase in surface area and surface density of active

2 sites.

3 Taking into account a relatively high activity, lower content of Ir and a comparatively low dissolution,

4 $Ir_{0.7}Sn_{0.3}O_{2-x}$ can be considered as an alternative anode material for application in the acidic OER. However,

5 electrochemical pretreatment of such electrodes leading to removal of Sn would probably be required to avoid

6 contamination of the membrane and the cathode catalyst with Sn. With an eye towards further decreases in Ir

7 utilization, materials containing less than 70 at.% of Ir should be tested also. One should keep in mind however, that

8 rutile IrO_2 with its at least two times lower initial dissolution rate is still a more stable material under conditions of the

9 OER. In case more stable materials are required, stoichiometric Ir-Sn oxide mixtures may be worthwhile to look at,

10 even though this implies sacrificing activity. The question of the OER activity and stability of other non-

11 stoichiometric and stoichiometric Ir-Sn mixed oxides will be addressed in following work.

12

13 **Conclusion**

14

15 The activity and stability relationship of reactively sputtered nonstoichiometric $Ir_{0.7}Sn_{0.3}O_{2-x}$ electrodes

16 during the OER was examined by the means SFC-ICP-MS and XPS. It was found that anodic polarization of the

17 electrode results in intensive preferential removal of Sn from the oxide matrix and formation of a porous Ir^{III}-

18 containing structure. The latter had a beneficial role for electrode performance as the activity increased significantly.

19 As an explanation for this phenomenon, an increase in surface area and/or the surface density of active sites was

20 suggested. Even though much lower, Ir dissolution was still observable and the measured rates were a factor of two

21 higher than that reported for rutile IrO_2. With time, the dissolution rate of both Sn and Ir decreased in a similar

22 manner. Additional long-term measurements in an h-cell revealed that the dissolution rate dropped after 1400 minutes

23 of electrolysis and steady state was established. The total amount of dissolved Ir in this time interval was still lower

24 than a single monolayer. On the other hand, more than ten monolayers of Sn were lost from the electrode. Owing to its

25 good electrode performance, the resulting material with an Ir-enriched surface can be considered as promising OER

26 catalyst.

27

28

29

4

References

6   [1] S. Trasatti, Electrochimica Acta, **29**, 1503-1512 (1984).
7   [2] R. Amadelli, A. Maldotti, A. Molinari, F.I. Danilov, A.B. Velichenko, Journal of Electroanalytical Chemistry,
8   **534**, 1-12 (2002).
9   [3] A.B. Velichenko, D.V. Girenko, N.V. Nikolenko, R. Amadelli, E.A. Baranova, F.I. Danilov, Russian Journal of
10 Electrochemistry, **36**, 1216-1220 (2000).
11 [4] N. Danilovic, K.E. Ayers, C. Capuano, J.N. Renner, L. Wiles, M. Pertoso, ECS Transactions, **75**, 395-402 (2016).
12 [5] S. Cherevko, S. Geiger, O. Kasian, A. Mingers, K.J.J. Mayrhofer, Journal of Electroanalytical Chemistry, **773**,
13 69-78 (2016).
14 [6] M. Carmo, D.L. Fritz, J. Mergel, D. Stolten, International Journal of Hydrogen Energy, **38**, 4901-4934 (2013).
15 [7] M. Schalenbach, G. Tjarks, M. Carmo, W. Lueke, M. Mueller, D. Stolten, Journal of The Electrochemical Society,
16 **163**, F3197-F3208 (2016).
17 [8] S.M. Alia, B. Rasimick, C. Ngo, K.C. Neyerlin, S.S. Kocha, S. Pylypenko, H. Xu, B.S. Pivovar, Journal of The
18 Electrochemical Society, **163**, F3105-F3112 (2016).
19 [9] S. Geiger, O. Kasian, B.R. Shrestha, A.M. Mingers, K.J.J. Mayrhofer, S. Cherevko, Journal of The
20 Electrochemical Society, **163**, F3132-F3138 (2016).
21 [10] T. Reier, Z. Pawolek, S. Cherevko, M. Bruns, T. Jones, D. Teschner, S. Selve, A. Bergmann, H.N. Nong, R.
22 Schlögl, K.J.J. Mayrhofer, P. Strasser, Journal of the American Chemical Society, **137**, 13031-13040 (2015).
23 [11] N. Danilovic, R. Subbaraman, K.C. Chang, S.H. Chang, Y. Kang, J. Snyder, A.P. Paulikas, D. Strmcnik, Y.T.
24 Kim, D. Myers, V.R. Stamenkovic, N.M. Markovic, Angewandte Chemie International Edition, **53**, 14016-14021
25 (2014).
26 [12] R. Kötz, S. Stucki, Electrochimica Acta, **31**, 1311-1316 (1986).
27 [13] V.A. Saveleva, L. Wang, W. Luo, S. Zafeiratos, C. Ulhaq-Bouillet, A.S. Gago, K.A. Friedrich, E.R. Savinova,
28 The journal of physical chemistry letters, 3240-3245 (2016).
29 [14] O. Kasian, S. Geiger, P. Stock, G. Polymeros, B. Breitbach, A. Savan, A. Ludwig, S. Cherevko, K.J.J.
30 Mayrhofer, Journal of The Electrochemical Society, **163**, F3099-F3104 (2016).
31 [15] O. Diaz-Morales, S. Raaijman, R. Kortlever, P.J. Kooyman, T. Wezendonk, J. Gascon, W.T. Fu, M.T.M. Koper,
32 Nature Communications, **7**, 12363 (2016).
33 [16] L.C. Seitz, C.F. Dickens, K. Nishio, Y. Hikita, J. Montoya, A. Doyle, C. Kirk, A. Vojvodic, H.Y. Hwang, J.K.
34 Norskov, T.F. Jaramillo, Science, **353**, 1011-1014 (2016).
35 [17] V.V. Gorodetskii, V.A. Neburchilov, Russian Journal of Electrochemistry, **41**, 971-978 (2005).
36 [18] S. Ferro, D. Rosestolato, C.A. Martínez-Huitle, A. De Battisti, Electrochimica Acta, **146**, 257-261 (2014).
37 [19] O.I. Kasian, T.V. Luk'yanenko, P. Demchenko, R.E. Gladyshevskii, R. Amadelli, A.B. Velichenko,
38 Electrochimica Acta, **109**, 630-637 (2013).
39 [20] O.I. Kasian, T.V. Luk'yanenko, A.B. Velichenko, Protection of Metals and Physical Chemistry of Surfaces, **49**,
40 559-566 (2013).
41 [21] I. Chiaki, I. Meguru, T. Hideo, Chemistry Letters, **8**, 225-228 (1979).
42 [22] D. Chen, C. Chen, Z.M. Baiyee, Z. Shao, F. Ciucci, Chemical Reviews, **115**, 9869-9921 (2015).
43 [23] T. Kishi, K. Shiota, Surface and Coatings Technology, **34**, 287-293 (1988).
44 [24] S.J. Freakley, J. Ruiz-Esquius, D.J. Morgan, Surface and Interface Analysis, (2017).
45 [25] V. Pfeifer, T.E. Jones, J.J. Velasco Vélez, C. Massué, R. Arrigo, D. Teschner, F. Girgsdies, M. Scherzer, M.T.
46 Greiner, J. Allan, M. Hashagen, G. Weinberg, S. Piccinin, M. Hävecker, A. Knop-Gericke, R. Schlögl, Surface and
47 Interface Analysis, **48**, 261-273 (2016).
48 [26] V. Pfeifer, T.E. Jones, J.J. Velasco Velez, C. Massue, M.T. Greiner, R. Arrigo, D. Teschner, F. Girgsdies, M.
49 Scherzer, J. Allan, M. Hashagen, G. Weinberg, S. Piccinin, M. Havecker, A. Knop-Gericke, R. Schlogl, Physical
50 Chemistry Chemical Physics, **18**, 2292-2296 (2016).
51 [27] A.A. Topalov, I. Katsounaros, J.C. Meier, S.O. Klemm, K.J. Mayrhofer, The Review of scientific instruments,
52 **82**, 114103 (2011).
53 [28] R. Kötz, H. Neff, S. Stucki, Journal of The Electrochemical Society, **131**, 72-77 (1984).
54 [29] H.G. Sanchez Casalongue, M.L. Ng, S. Kaya, D. Friebel, H. Ogasawara, A. Nilsson, Angewandte Chemie
55 International Edition, **53**, 7169-7172 (2014).

[30] L. Kövér, Z. Kovács, R. Sanjinés, G. Moretti, I. Cserny, G. Margaritondo, J. Pálinkás, H. Adachi, Surface and Interface Analysis, **23**, 461-466 (1995).

[31] Q. Ni, D.W. Kirk, S.J. Thorpe, Journal of The Electrochemical Society, **162**, H40-H46 (2015).

[32] J. Augustynski, M. Koudelka, J. Sanchez, B.E. Conway, Journal of Electroanalytical Chemistry and Interfacial Electrochemistry, **160**, 233-248 (1984).

[33] S. Cherevko, S. Geiger, O. Kasian, A. Mingers, K.J.J. Mayrhofer, Journal of Electroanalytical Chemistry, **774**, 102-110 (2016).

[34] J.Y. Ying, A. Tschöpe, Chapter 10 - Gas-Phase Synthesis of Nonstoichiometric Nanocrystalline Catalysts A2 - Moser, William R, Advanced Catalysts and Nanostructured Materials, Academic Press, San Diego, 1996, pp. 231-257.

[35] A. Daghetti, G. Lodi, S. Trasatti, Materials Chemistry and Physics, **8**, 1-90 (1983).

[36] M. Pourbaix, Atlas of electrochemical equilibria in aqueous solutions, (1974).

[37] S. Cherevko, T. Reier, A.R. Zeradjanin, Z. Pawolek, P. Strasser, K.J.J. Mayrhofer, Electrochemistry Communications, **48**, 81-85 (2014).

[38] M.K. Debe, Nature, **486**, 43-51 (2012).

[39] S. Cherevko, S. Geiger, O. Kasian, N. Kulyk, J.-P. Grote, A. Savan, B.R. Shrestha, S. Merzlikin, B. Breitbach, A. Ludwig, K.J.J. Mayrhofer, Catalysis Today, **262**, 170-180 (2016).

1   **Figures**

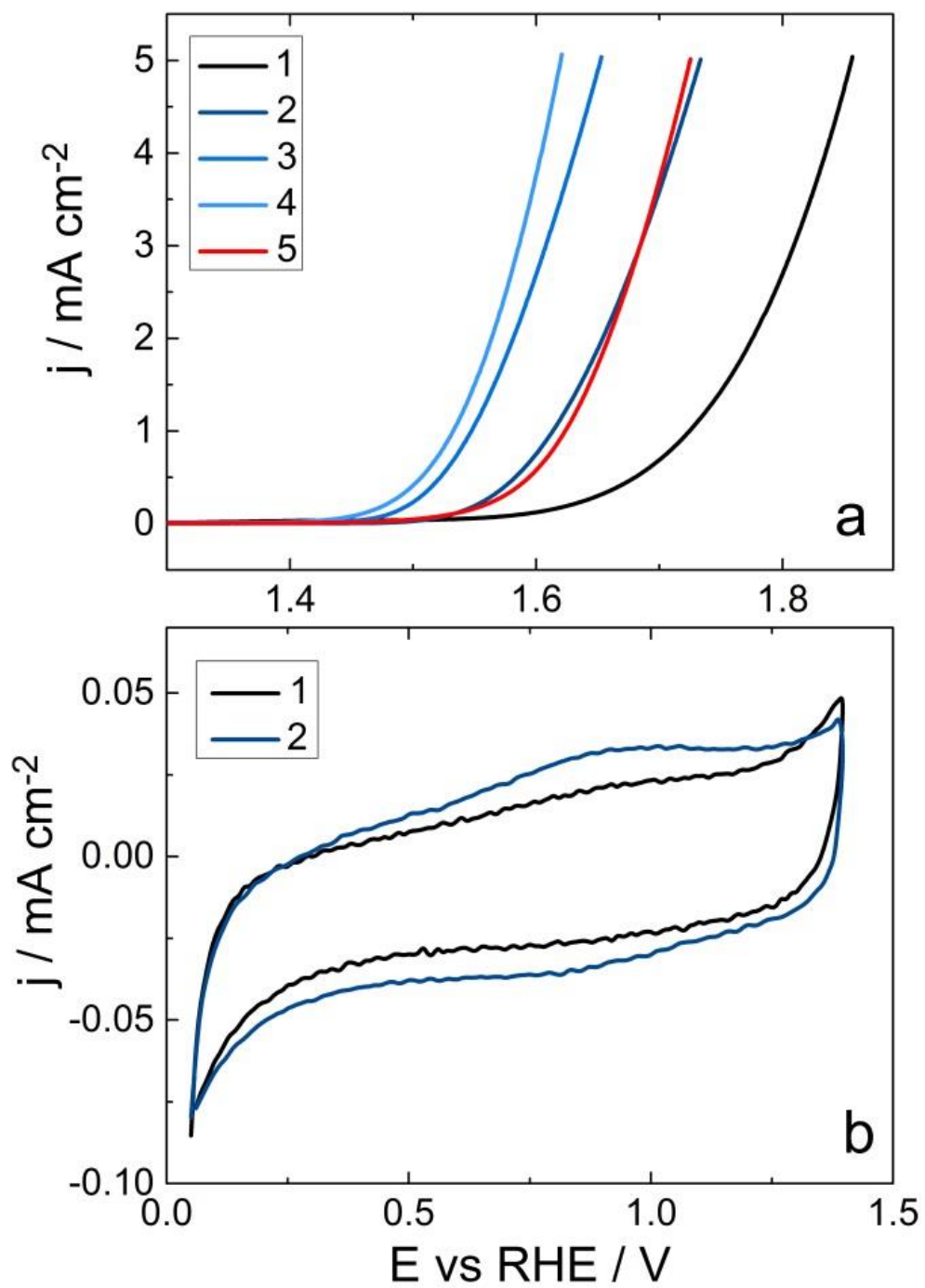2   **Fig. 1.**
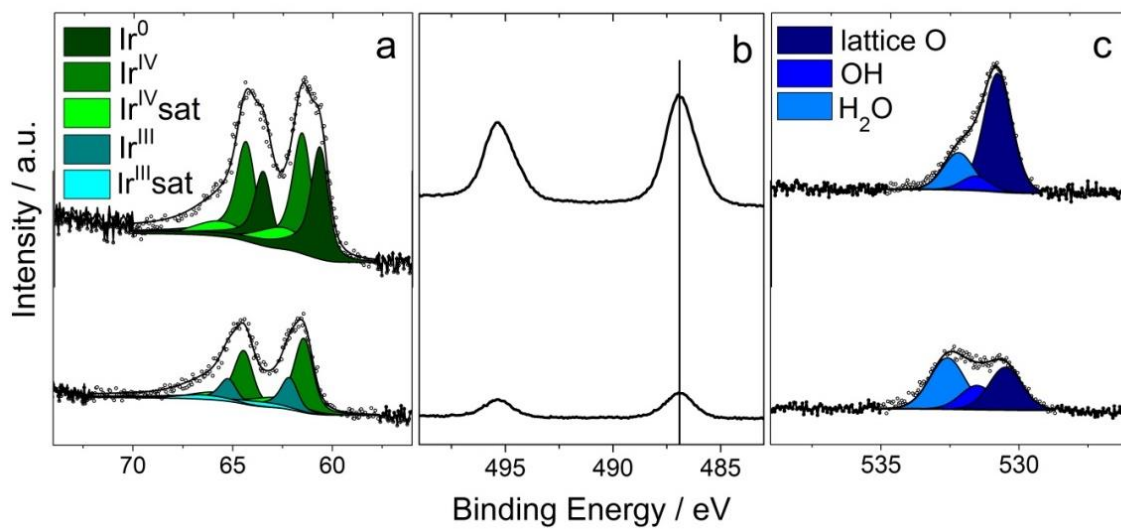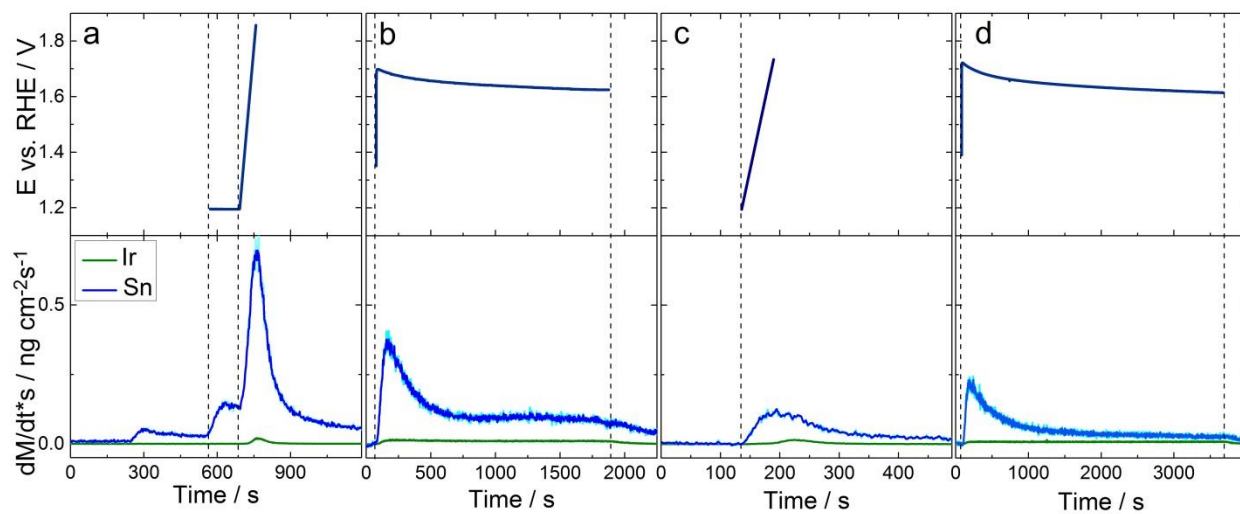

3
4
5
6
7
8
9
10
11
12
13
14
15
16
17
18
19
20
21
22

1   **Fig. 2.**
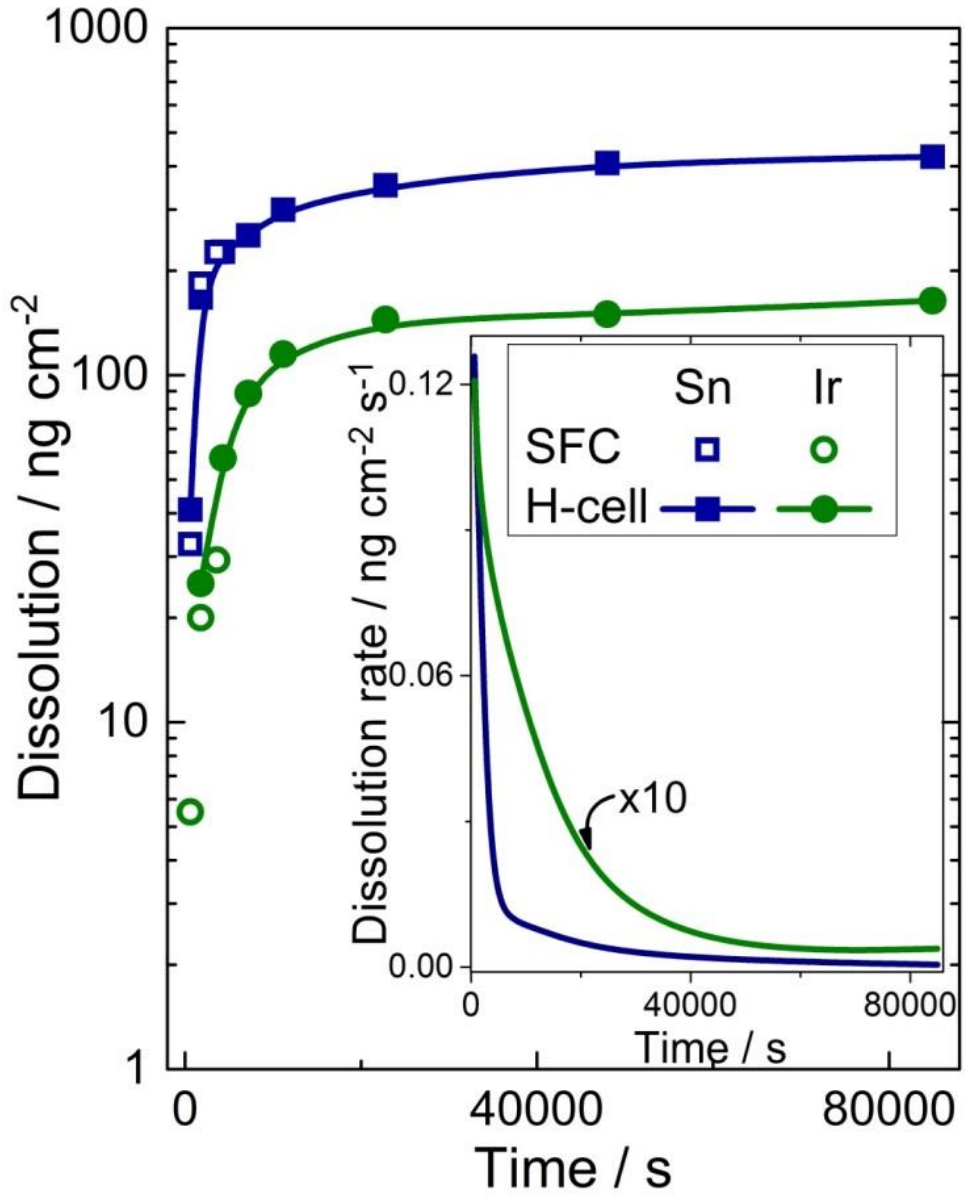

2

3

4

5

6

1 **Fig. 3.**

1   **Fig. 4.**

2

3

4

5

1   **Figure captions**

2

3   **Fig. 1.** XP spectra of Ir 4f (a), Sn 3d (b) and O 1s (c) levels for the as-prepared $Ir_{0.7}Sn_{0.3}O_{2-x}$ electrode (top

4 curves) and after its anodic polarization over 1 hour in 0.1 M $HClO_4$ at 1 mA cm^{-2} (bottom curves).

5

6   **Fig. 2.** Electrochemical characterization of as-prepared $Ir_{0.7}Sn_{0.3}O_{2-x}$ electrode (1) and after 30 (2), 60 (3) or

7 1400 min (4) of anodic polarization in 0.1M $HClO_4$ at 1 mA cm^{-2}. (a) The quasi-steady-state anodic polarization

8 curves measured during potential scan from 1.2 V_{RHE} until the potential corresponding to the current density of 5 mA

9 cm^{-2} is reached. The scan rate was 10 mA cm^{-2}. For comparison, data for stoichiometric IrO_2 is added from Ref.[14]

10 (5). (b) Cyclic voltammograms of as-prepared and 60 min. polarized $Ir_{0.7}Sn_{0.3}O_{2-x}$ electrodes, taken in the range of

11 0.05 − 1.4 V_{RHE} with a scan rate of 50 mV s^{-1}. All presented measurements were performed in the SFC-ICP-MS set-

12 up.

13

14   **Fig. 3.** The applied (a, c) and measured (b, d) potential (upper pane) and corresponding dissolution rates

15 (lower pane) plotted vs. time for an $Ir_{0.7}Sn_{0.3}O_2$ electrode. The potential was scanned (a, c) from 1.2 V_{RHE} to the

16 potential corresponding to a current density of 5 mA cm^{-2} with a scan rate of 10 mV s^{-1}, then measured (b) during 30

17 or 60 min. (d) of anodic polarization at 1 mA cm^{-2}. In (c) the material was re-scanned identically to (a) after the

18 anodic polarization.

19

20   **Fig. 4.** Dependence of amount of dissolved Ir and Sn during anodic polarization at 1 mA cm^{-2} in 0.1 M

21 $HClO_4$ using SFC (opened symbols) or h-cell with divided anodic and cathodic compartments (closed symbols) on

22 electrolysis time. The inset shows the corresponding variation of dissolution rate with time of electrolysis.

23

24